AD-A031 007 TEXAS TECH UNIV LUBBOCK DEPT OF ELECTRICAL ENGINEERING F/G 19/1
RADIATION GENERATION FROM EXPLODING WIRE.(U)
AUG 76 M G BHATTACHARYA, J P CRAIG, T F TROST AF-AFOSR-2830-75
UNCLASSIFIED AFOSR-TR-76-1105 NL

1 OF 1
AD A031007

END
DATE FILMED
11-76

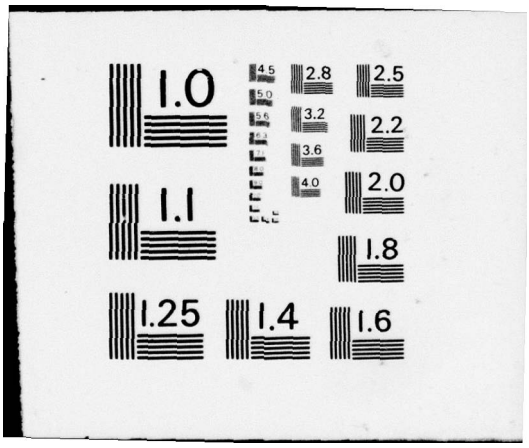
1.0
1.1
1.25
1.4
1.6
1.8
2.0
2.2
2.5
2.8
3.2
3.6
4.0
4.5
5.0

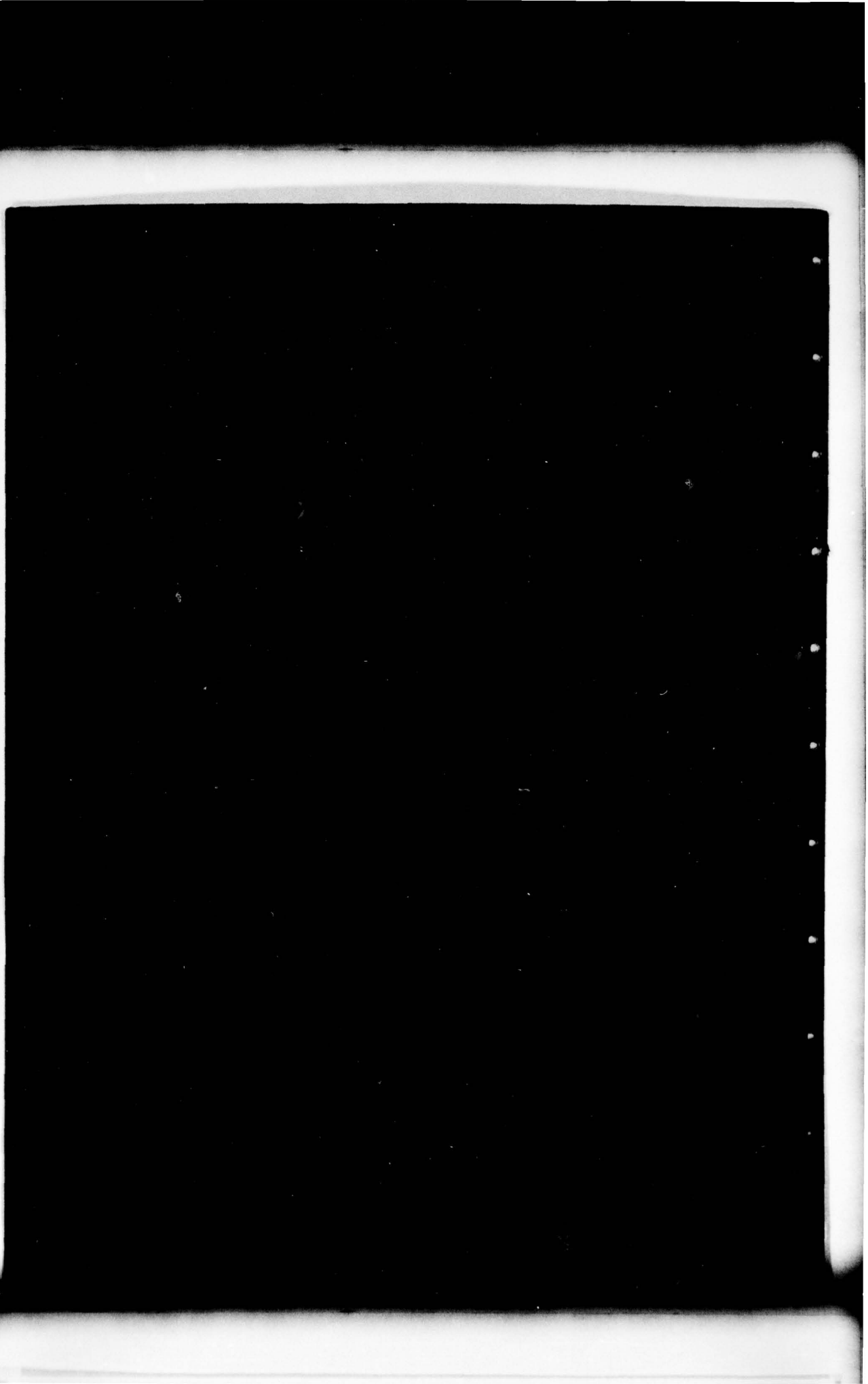

CHAPTER I

INTRODUCTION

Exploding wires with high current pulses have been studied for about two decades.[1] In recent years pulsers capable of delivering on the order of terrawatts of power for tens of nanoseconds have become available.[3] These high power pulsers have been used to produce electron beams[4] and to explode wires.[5]

The Gamble II generator, for example, consists of a Marx generator which stores 228 kJ, an intermediate storage capacitor, a pulse forming line and a coaxial impedance transforming line with an output impedance of 1.5 ohms. It has been used to deliver on the order of 40 kJ to an exploding tungsten wire.[5,6]

Although such a device produces tens of Joules of radiation in the soft X-ray spectrum, it is of interest to examine the possibility of scaling the technique to higher power levels. The usefulness of a scaled-up power supply to increase the soft X-ray radiation depends upon how well the resulting plasma load matches the high power pulser.

Exploding Wire Plasma Load Characteristics

Mosher, et al, have reported that "appropriate" plasma loads tend to match to the generator driving them.[5] This was found to be true for tungsten wires on the order of 25μ diameter, 3 to 4 cm in length, open circuit power supply voltages, v_o, in the range 2-5 MV. It remains to be seen whether or not the matching will extend to appreciably higher power levels.

The power supply, or pulser, is adequately represented by a voltage source and a resistance for the time period of interest. The exploding wire and its mounting jig can be represented, insofar as its effect on the circuit is concerned, by a time varying series R-L impedance. The circuit is shown in Fig. 1.

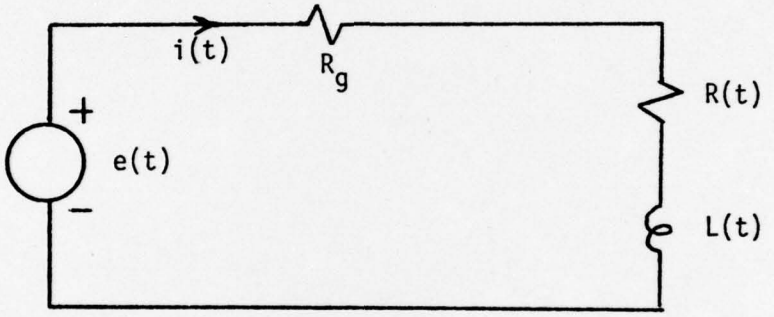

Fig. 1 Equivalent circuit for exploding wire pulser

The simplicity of the circuit in Fig. 1 is highly misleading, since the innocent looking terms L(t) and R(t) are actually extremely complicated functions of the exploding wire plasma parameters. The plasma parameters, in turn, are sensitive to the voltages and currents in Fig. 1. Because of the complex non-linearities involved, any theoretical treatment of the problem must involve computer aided numerical solutions for specific cases. To date, no computer program is available which describes how the exploding wire plasma reacts.

A one-dimensional code has been reported[5] which includes the radiation and electron transport equations, Maxwells equations and the external circuit. This code is a significant piece of work which

utilizes the Corona equilibrium model[7] to describe the local high-temperature properties of the plasma. Although the results obtained with this code agree, in a broad brush sense, with the experiments performed to date with power levels on the order of a terrawatt, the authors point out that the effect of run-away electrons has not been included. And, of course, since it is one-dimensional, it does not include the effects of the observed m = 0 instabilities.

Apparently, the run-away electrons are created in the low density regions at the surface of the plasma cylinder. Chapter II of this report considers the radiation from the time varying, non-Maxwellian velocity distribution which developes in a plasma in the presence of a strong electric field. The remainder of Chapter I discusses in a semi quantitative manner the load R(t) and L(t) characteristics, the m = 0 instability and the scaling up problem.

Kirchhoff's voltage equation for Fig. 1 may be written

$$e(t) = [R_g + R(t)]\, i(t) + \frac{d}{dt}\,[L(t)i(t)] \qquad (1)$$

The inductance is the ratio of the flux within the plasma plus the flux within the jig but outside the plasma to the current. This inductance varies with time for two reasons. First, the flux per unit current within the plasma varies because the current density distribution and the radius of the plasma both vary. Second, the flux outside the plasma per unit current varies because the plasma radius varies. (It is not clear from the reference cited above that this second L variation was included in the one-dimensional code, although it may have been.) It will be seen that the variation due to the second reason are larger than those due to the first.

Consider the inductance due to the flux inside a cylindrical plasma with a 2 mm radius, r_o, and 4 cm long, with the current uniformly distributed,

$$L = (1/2 \times 10^{-7})(0.04) = 2 \times 10^{-9} \text{ hy} \qquad (2)$$
$$= 2 \text{ nhy}.$$

Now if the plasma is compressed to 0.05 mm radius, r_p, the inductance becomes

$$L = 2 \times 10^{-9} + 2 \times 10^{-7} \ell \ell n \frac{r_o}{r_p} \qquad (3)$$
$$= 2 + 2(\ell n\ 40) = (2 + 7.38) = 9.38 \text{ nhy}$$

If the current density within the plasma is higher near its outer radius and lower near its center, the inductance in eq. (1) and the first term in eq. (2) are even smaller than 2 nhys.

If the diameter of the wire were 25μ, the inductance due to the flux inside a 4 cm cylinder out to a radius of 2 mm is 12.15 nhy. If the wire explodes and the plasma expands to a 2 mm radius, the inductance drops from 12.15 nhy to less than 2 nhys if the current density is larger near the plasma surface. In the process of this expansion, some plasma energy is removed and fed into the magnetic field. If the plasma is subsequently compressed to a radius of 0.05 mm, the inductance goes back up to a value between 7.38 and 9.38 nhy, depending upon the current distribution. During the compression, some magnetic field energy is converted into plasma energy.

Of course, there is an additional inductance due to the flux within the jig, but outside the 2 mm radius, (~50 nhy) which must be added to

the above inductances to obtain the L(t) for eq. (1). Numerical solutions of eq. (1) with typical R(t) and L(t) values and with e(t) a step function of 2 MV, and $R_g = 1\Omega$, gives a current which rises to the order of 1 MA in a few tens of nanoseconds. In some cases the current does not monotonically increase, but has a slight dip in the region where dL/dt is positive. However, since the current is higher during the compression stage than during the expansion stage, a net energy of the order of a kilojoule can be fed into the plasma.

The effective resistance of the plasma is very important, since most of the heating is due to the I^2R loss within the plasma. Examination of the approximate resistance of a 4 cm long, 25μ diameter tungsten wire as a function of temperature is enlightening. The resistivity of tungsten[8] at 300°K is 5.65 μ ohm cm and rises to 117.1 at 3655°K. The wire resistance goes from 4.6 up to 95 ohms as the temperature increases from room to melting temperature. The effective resistance of the wire load may not reach a value as high as 95 ohms since some thermionic electrons will be emitted. Also, no data is available for the resistance of the tungsten during the time that it is being vaporized and ionized. Fortunately, the value of resistance during this time frame does not appear to be too critical insofar as the high temperature matching problem is concerned. For example, if the plasma resistance, R(t) in Fig. 1 were 10 ohms, then a large fraction of the generator voltage would be dropped across R(t). A voltage of say 500 kV, would produce a power of 25 Gw, which would represent an energy of 250 joules in 10 ns. Since only a few tens of joules are

needed to vaporize and ionize the tungsten once or twice, a resistance between 10 and 100 ohms would only last for 10 to 20 ns at most.

The resistivity of the ionized plasma above about 10^5 °K can be calculated from equations from Spitzer's book.[9] In the absence of a magnetic field the plasma resistiveity is given by

$$\eta = 3.8 \times 10^3 \frac{Z \ell n\Lambda}{\gamma_E T^{3/2}} \text{ ohm - cm}, \qquad (4)$$

where Z is the ionic charge, γ_E is a factor given in Table 1, T is the temperature in °K, and $\ell n\Lambda$ is given in Table 2.

Table 1 Factor γ_E for equation (4)

Ionic Charge	1	2	4	16	∞
γ_E	0.582	0.683	0.785	0.923	1.000

Table 2 Values of $\ell n\Lambda$ for equation (4)

		Ion density (cm^{-3})		
Temp.	<Z>	10^{18}	10^{19}	10^{20}
10^5	6	5.79	4.64	3.49
10^6	11	7.79	6.64	5.49
10^7	47	9.37	8.22	7.06
10^8	63	11.52	10.37	9.22

The average values of Z in Table 2 are obtained from Mosher.[7]

In a strong magnetic field transverse to the electric field,

the resistivity becomes

$$\eta_{\perp} = 1.29 \times 10^{4} \frac{Z \ell n \Lambda}{T^{3/2}} \text{ ohm - cm} \qquad (5)$$

The calculations below indicate that a strong transverse magnetic field exists near the plasma surface at high temperatures and currents, but not in the central regions of the plasma.

The magnetic induction at the surface of a plasma cylinder of radius r is $\mu_o I/2\pi r$, which yields 10 tesla with 0.1 MA at r = 2 mm. Since the observed radii are in the range of 0.1 to 1 mm for currents on the order of 1 MA, there is a strong magnetic field near the surface of the plasma. The resistivities for a tungsten plasma with ion densities of 10^{18} and 10^{20} cm^{-3} with a strong transverse magnetic field are given in Table 3.

TABLE 3 Resistivity of Tungsten Plasma in a Strong magnetic field. (ohm - cm)

T °K	$n_i = 10^{18}$ cm^{-3}	$n_i = 10^{20}$ cm^{-3}
10^5	1.42×10^{-2}	8.54×10^{-3}
10^6	1.11×10^{-3}	7.79×10^{-4}
10^7	1.80×10^{-4}	1.35×10^{-4}
10^8	9.36×10^{-6}	7.49×10^{-6}

The resistance of the plasma would be given by

$$R_{D-C} = \eta \frac{\ell}{A} \qquad (6)$$

if the current were uniformly distributed over the plasma cross section. However, the resistivity is sufficiently low and the time period of the

current pulse is sufficiently short, that the skin effect may be appreciable. The skin effect on the plasma resistance can be taken into account by using the skin depth from Table 4, the ratio of r/δ from Table 5 and the ratio of R/R_{D-C} given in Fig. 2.

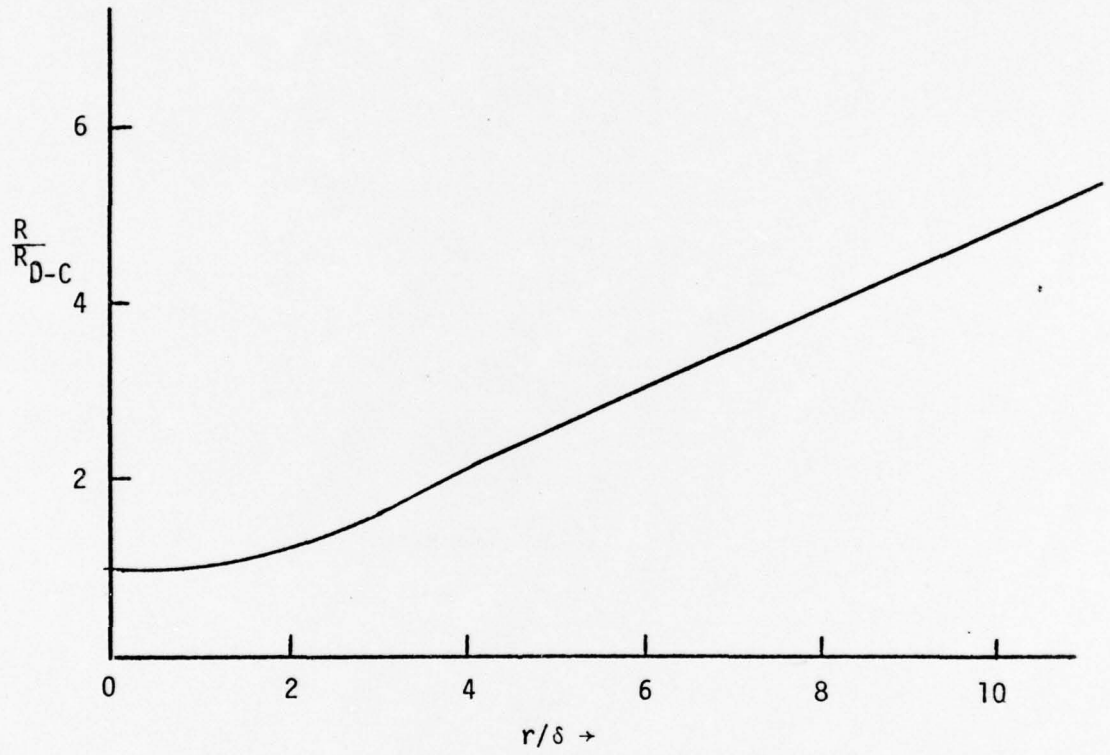

Fig. 2 Skin Effect Factor

The resulting resistances for a tungsten plasma cylinder with three different radii are plotted in Fig. 3. The curve line widths represent variations in ion density form 10^{18} to 10^{20} cm^{-3}, and use the resistivity values for strong transverse magnetic fields. The resistance curve for low temperature is for the tungsten wire

TABLE 4 Skin depth, $\delta = \sqrt{\frac{\eta}{\pi f \mu}}$

T °K	for $n_i = 10^{18}$ cm^{-3} mm	$n_i = 10^{20}$ cm^{-3} mm
10^5	0.560	0.465
10^6	0.168	0.141
10^7	0.067	0.058
10^8	0.015	0.014

TABLE 5 Ratio of radius to skin depth, r/δ

	for $n_i = 10^{18}$ cm^{-3}			$n_i = 10^{20}$ cm^{-3}		
T °K	R = 2 mm	0.5 mm	0.05 mm	2 mm	0.5 mm	0.05 mm
10^5	3.57	0.89	0.089	4.3	1.08	0.108
10^6	11.9	2.97	0.297	14.2	3.55	0.355
10^7	29.8	7.46	0.746	34.5	8.62	0.862
10^8	13.3	33.3	3.33	14.3	35.7	3.57

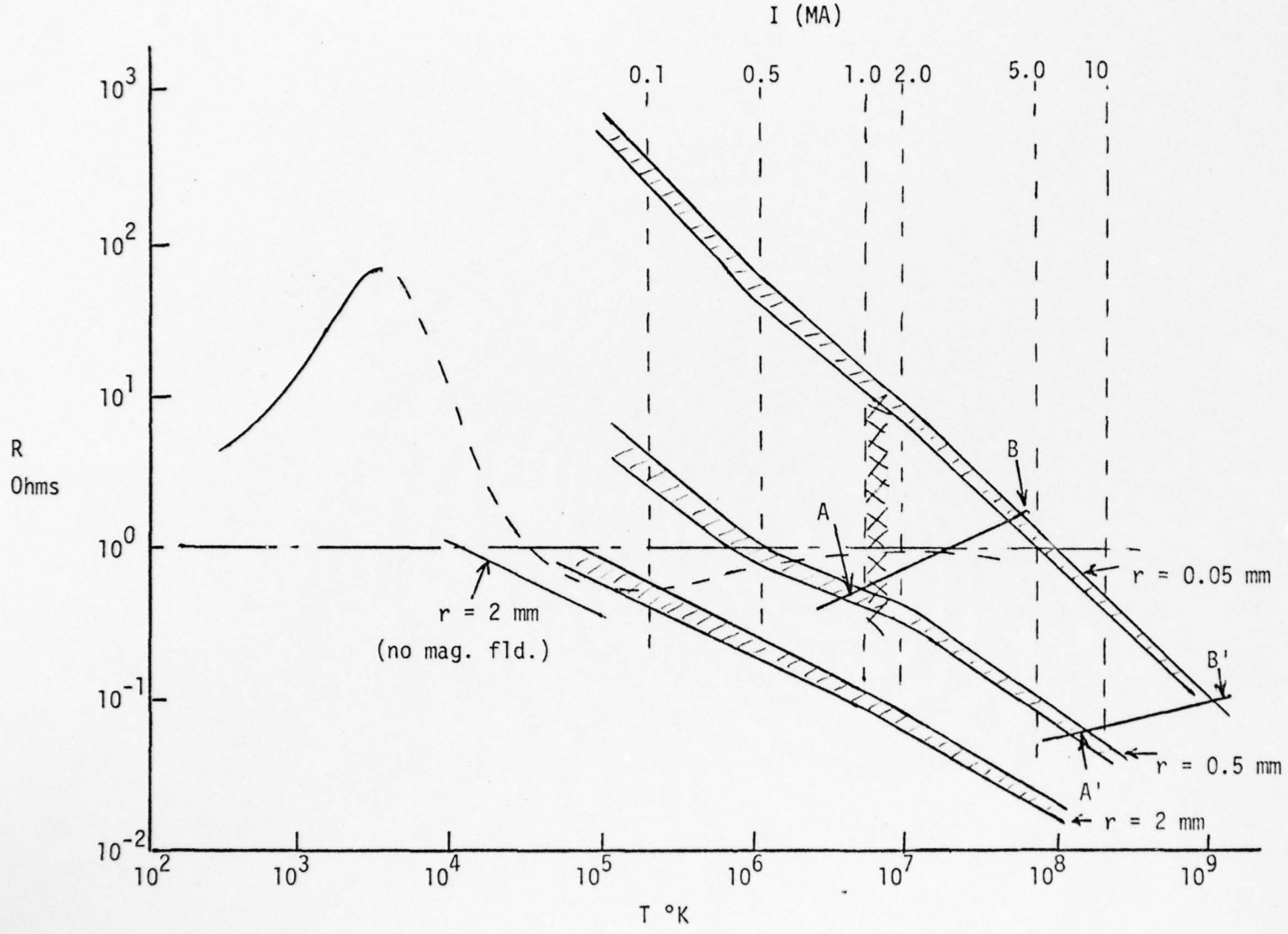

Figure 3 Resistance of exploded Tungsten, 25μ diameter, by 4 cm long wire.

before it melts. The dotted extension of this curve to higher temperatures is an estimate. The lowest resistance curve for the 10^4 to 10^5 temperature range is for a plasma of 2 mm radius and no magnetic field. After the plasma is compressed and is in a quasi-equilibrium condition, the kinetic pressure and the magnetic field pressure are approximately equal at the plasma surface. That is

$$\frac{N_i}{\pi r^2 \ell} [1 + \langle Z \rangle] kT = \frac{\mu_o I^2}{8\pi r^2} \qquad (7)$$

Equation (7) is independent of r, hence m = 0 instability can easily develop. If N_i/ℓ remains constant, as it does in the one dimensional code, the temperature necessary to balance different currents can be calculated from eq. (7) and are plotted as the vertical dashed lines in Fig. 3.

The cross-hatched area on Fig. 3 represents the range of R values which would be obtained if the plasma reached a semi-equilibrium radius between 0.5 and 0.05 mm with 1 to 1.5 MA through the plasma. Note the 1.5 Ω Gamble II impedance is near the center of this range. The corresponding equilibrium temperature is 7-8 x 10^6 °K.

However, time integrated X-ray photographs experimentally obtained with hv > 2 keV indicate an m = 0 instability with the plasma dimensions as indicated in Fig. 4.

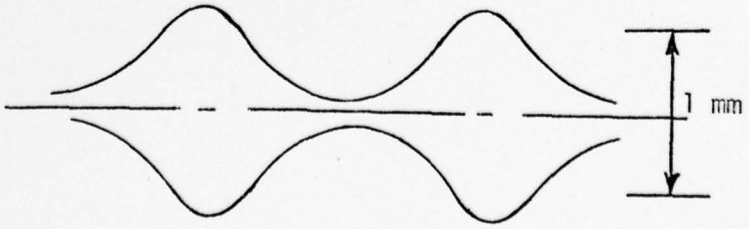

Fig. 4 A portion of the plasma column shape as indicated by X-ray photograph

The effect of the m = 0 instability can be semi-quantitavely understood by considering the plasma shape shown in Fig. 5.

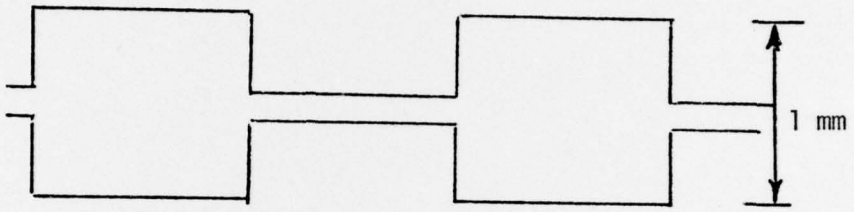

Fig. 5. Hypothetical plasma column shape

If there were no net transport of the ions and electrons in the z-direction, the ion density in the larger diameter area would be ~ 4×10^{19} and in the small diameter area ~ 4×10^{21} cm^{-3}. But this would result in a very large density gradient in the z-direction over a distance of the order of the difference in radii, so no transport of the ions in the z-direction is hardly possible -- especially near the center of the column where it will be seen that the magnetic field is low. Therefore, the ion density in the small diameter region is probably closer to 4×10^{20} cm^{-3} than 4×10^{21}. This decrease in ion density would cause an increase in the ion density in the larger diameter region to ~ 7×10^{19} cm^{-3}. The change in ion density in the small diameter region would call for an increase in the term $(1 + \langle Z \rangle)T$ on the left hand side of eq. (7) by a factor of 10 to balance the same current and its corresponding magnetic field. Since $\langle Z \rangle$ at the high temperature will increase

~25%, the temperature in the small diameter region near the plasma surface would be ~ 5-6 x 10^7 °K. Similarly, the higher density in the larger diameter region would need a temperature of ~ 4 x 10^6 °K to maintain the semi-equilibrium condition. These two conditions are marked by points A and B on Fig. 3. If 50% each of the plasma column length is the small and the large diameter, the total resistance would be the average of the two values for A and B, or approximately 1 ohm. For the observed shape shown in Fig. 4, the resistance would be expected to be an average value of the straight line through A and B. This is reasonably close to experimental observations.

Also, X-radiation spectra measurements on a plasma similar to that discussed here indicate temperatures on the order of 5 x 10^7 °K are obtained.[6]

For the conditions along the line through A and B the ratio of the radius to the skin depth δ is ~ 3. Therefore, current density near the surface of the plasma is on the order of 3 times that at the center of the plasma. This higher current density, together with the higher resistivity in the strong magnetic region means that the heating rate near the surface is ~ 10 times that near the center. Since the radiation is higher for the hotter regions near the surface, a temperature ratio of less than 10 between the surface and center regions of the plasma would be expected. Therefore, the ions near the center of the larger diameter regions are probably less than 10^6 °K.

Since the plasma at the surface will diffuse radially into the magnetic field, there will be a low density region near the surface of the plasma. Conditions for run-away electrons can occur in this

region. Those that are produced near the surface of the smaller diameter regions would move along the z-direction into the low temperature core regions of the larger diameter plasma. This can account for the strong L-line emission which has been experimentally observed.

A rough check on the energy required to yield the temperatures estimated above can be obtained using the specific heats given by Mosher.[7] This is found to be ~ 25 kJ, or a little over half the 40 kJ that are deposited in the plasma. The remainder of the energy is radiated both during the time the temperature distribution is being developed, as well as the time period after the semi-equilibrium condition is reached.

Since the above model appears to check fairly well with the salient features found experimentally, it may shed some light on the possibility of scaling to high power levels.

Fig. 3 is useful to understand how the plasma parameters will change for increased power levels. For a current of 10 MA the vertical dotted line indicates that the magnetic field and the kinetic pressure will be in equilibrium at ~ 2×10^8 °K, with no variation in N_i/ℓ with z. With an $m = 0$ instability the points A' and B' are approximated in the same manner that A and B were obtained for the lower current. The resistance of the plasma would then be an average of points along the A'B' line. It is likely that the equilibrium radii will be less than those for the lower current, but it appears from Fig. 3 that the resistance will still be ~ 0.1Ω. With the current up by a factor of 10 and the resistance down by a factor of 10, the i^2R heating would be up by a factor of 10. For semi-equilibrium, the radiation must then be up by a factor of 10.

The radiation rates are given by[7]

$$P_c = 1.62 \times 10^{-30} \sqrt{T}\ \langle Z \rangle\ n_i^2 [\langle Z \rangle + \langle \frac{Z^2 x_{Z-1}}{T} \rangle] \text{ w/cm}^3 \quad (8)$$

and

$$P_L = 3.77 \times 10^{-23} \sqrt{T}\ \langle Z \rangle\ n_i^2 < \exp[\frac{E^Z n_1}{T}] > \text{ w/cm}^3 \quad (9)$$

where, P_c is the continuum radiation, P_L is the line radiation in the absence of trapping and the bracket term is equation 8 is given in reference 7. Since these terms only increase as the $\sqrt{T}$, and $\langle Z \rangle$ increase only a few per cent, n_i must go up slightly to increase the radiation by a factor of 10. This is consistant with the assumption that the average radii will be slightly smaller than for the lower current case. Therefore, it appears that if the current is increased by a factor of 10, the radiation will increase by approximately 10.

However, it is important that the scaled-up current still have a time scale comparable to that for the lower current case. If the current rise time is extended, the skin depth will be greater and the plasma resistance will be even less than ~ 0.1 ohm. If the generator impedance were reduced by a factor of 10 and the jig inductance is not reduced, the current would be much longer in reaching its value, and the resulting increase in temperature and radiation would be less. On the other hand, if the generator were scaled up in voltage and the generator resistance and jig inductance held constant, the current rise time would increase only slightly. Of course, it may be difficult to hold the jig inductance down with the scaled up generator voltage. Also, a smaller per centage of the initial power supply energy will be supplied

to the plasma. Probably a compromise between a scaled-up voltage and a scaled down generator impedance would be the optimum to obtain the higher current. The determination of the optimum generator involves considerable study which is beyond the scope of this report.

CHAPTER II

PLASMA BREMSSTRAHLUNG CALCULATIONS

In this section we compute the bremsstrahlung spectrum for a high temperature plasma in a strong electric field. Our interest is in obtaining a theoretical framework for comparison with the measured spectrum of Mosher et al.[6] for an exploded-wire discharge. Our approach is quite restricted and is not an attempt to describe all the very complex physics of an exploded wire plasma. Basically, we have integrated the time-dependent electron velocity distribution of Kovrizhnykh[10] together with the classical bremsstrahlung cross section with the results of Grant[11] for the Gaunt factor. The calculations show a systematic flattening out of the spectrum with time as the electron velocity distribution is shifted and distorted from an initial maxwellian shape by the electric field. This flatness is a feature which is also seen in the experimental exploded-wire spectrum.

Before describing the bremsstrahlung emitted by plasma electrons which have a distribution of velocities, we consider the simpler case of the bremsstrahlung from mono-energetic electrons.

As the electrons encounter positive ions, they scatter and emit bremsstrahlung over a broad frequency spectrum. Close encounters result in large scattering angles and the radiation of high frequencies while more distant encounters give mild deflections and lower frequency radiation. To calculate the radiation one should use a quantum mechanical analysis when the de Broglie wavelength of the electron is comparable to the typical impact parameter. This regime is specified by

$$E > 13.6\bar{z}^2 \text{ eV}, \qquad (10)$$

where E is the kinetic energy of the electron ($1/2\ mv_o^2$) and $\bar{z}$ the atomic number of the ion. For smaller values of E a classical analysis can be applied. In the classical case the bremsstrahlung is given by[11,12]

$$X(w) = \underbrace{\frac{4e^2 b_o^2 v_o^2}{3\sqrt{3}\varepsilon_o c^3}}_{S_o(v_o)} \underbrace{\frac{\pi\sqrt{3}}{4}\, u_o\, H_{u_o}^{(1)}(u_o)\left\{\frac{d}{du}\left[H_{u_o}^{(1)}(u)\right]\right\}_{u=u_o}}_{G(w,v_o)}, \qquad (11)$$

where X(w) is the cross section for radiation in the range w to w + dw. It has units of joules - m^2/rad./sec. Also $u_o = \frac{wb_o}{v_o}$, $b_o = \frac{\bar{z}e^2}{4\pi\varepsilon_o m v_o^2}$, and $H_{u_o}^{(1)}$ is the Hankel function of the first kind and order u_o. $G(w,v_o)$ is the Gaunt factor and contains the dependence of the radiation on frequency. It is of order unity. There are two restrictions on this formula: 1) $w \gg w_p$ = plasma frequency, in order to be able to neglect collective motions of the electrons; and 2) $\hbar w \ll \hbar w_{max} = 1/2mv_o^2$, since the formula is derived assuming negligible energy is carried away by the photon.

Applied to tungsten wires ($\bar{z} = 74$) for comparison with the exploded-wire discharge, equation 10 gives E>76.5 keV for the quantum mechanical regime. Here we use the Born-Elwert formula,[12,13]

$$X(w) = S_o(v_i)\,\frac{\sqrt{3}}{\pi}\,\frac{\eta_2}{\eta_1}\left[\frac{1-e^{-2\pi\eta_1}}{1-e^{-2\pi\eta_2}}\right]\ell n\left[\frac{\overline{m}(v_i-v_f)^2}{2\hbar w}\right], \qquad (12)$$

where $\eta_1 = \frac{\bar{z}e^2}{4\pi\varepsilon_o \hbar v_i}$, $\eta_2 = \frac{\bar{z}e^2}{4\pi\varepsilon_o \hbar v_f}$, and v_i and v_f are the electron

speeds before and after collision, respectively. This formula allows for the energy carried away by the photon ($\hbar w = 1/2mv_i^2 - 1/2mv_f^2$). The restrictions are $w << w_{max}$ and non-relativistic electron energy.

In Fig. 6 we have plotted X(w) for 5 different electron energies, using the appropriate formula, either equation 11 or 12, as indicated in Table 6. It is clear from the figure that the bremsstrahlung spectra are quite flat and have about the same slope for all of the electron energies considered. So by merely observing that the spectrum is flat in a particular experiment one could not learn the electron energy. One would need to determine the high-frequency cutoff of the spectrum or perhaps examine the X-ray line emission.

Curves like those in Fig. 6 for target ions other than tungsten can be generated by using equation 11 for electron energies $E < 13.6\bar{z}^2$ and equation 12 for $E > 13.6\bar{z}^2$. Since the equations are non-relativistic, E should be kept below the electron rest mass, $mc^2 = 511$ keV. Koch and Motz[13] discuss what happens if E is greater than this.

A correction that has not been included in the spectra of Fig. 6 is that due to the screening of the ion nucleus by any remaining bound electrons. We cannot restrict the analysis to only fully ionized species, since for the tungten exploded-wire plasma this is not the case. The screening alters the spectra in the range of frequencies below the frequency w_s, where[14]

$$\frac{w_s}{w_{max}} \sim \frac{\bar{z}^{1/3}}{96} \frac{c}{v}$$

If included, it would merely flatten the low-frequency end of the spectrum, whereas in Fig. 6 the spectrum gradually rises with decreasing frequency.

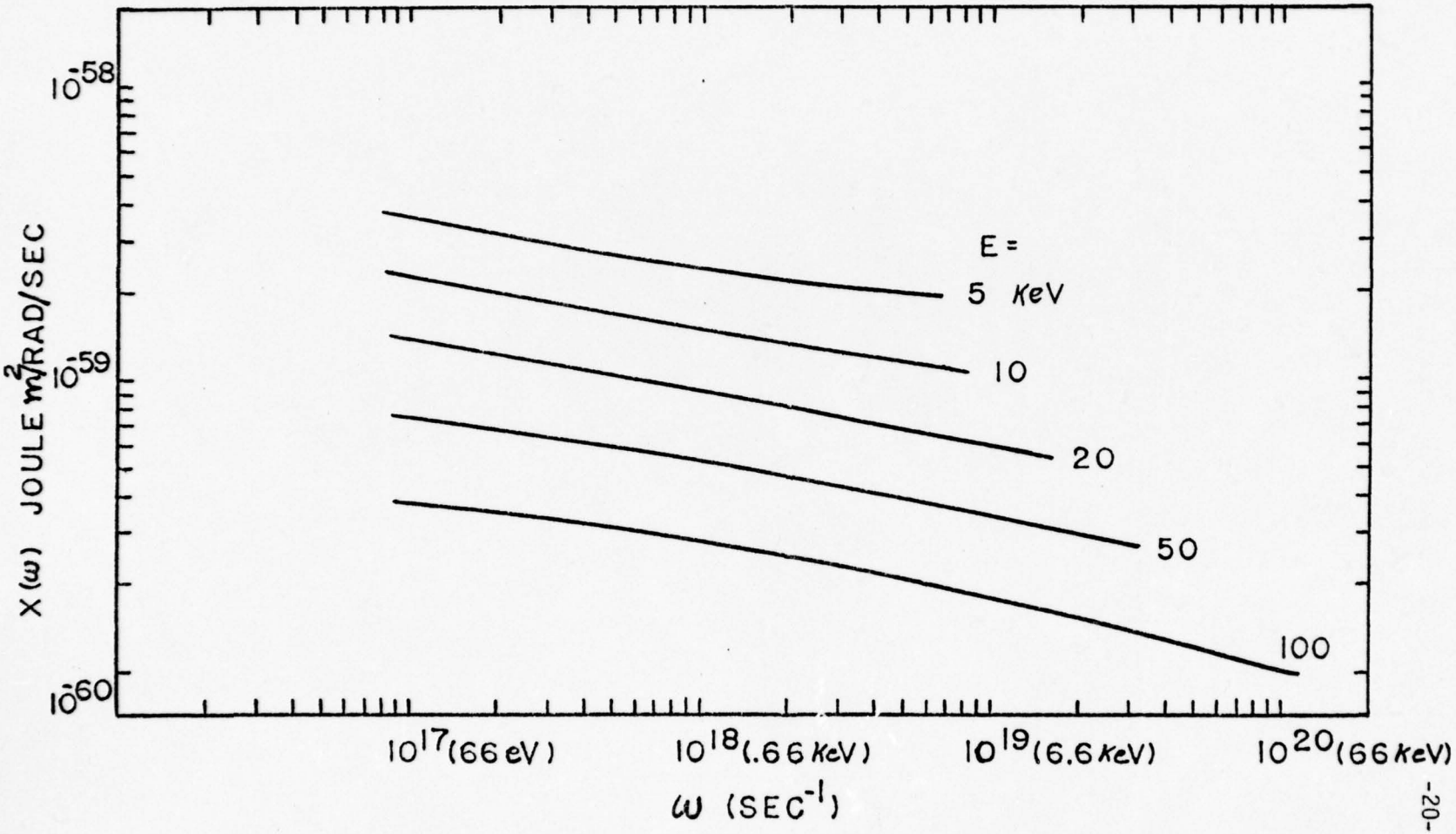

Figure 6. Bremsstrahlung spectra for various electron energies, E.

Note that in the exploded-wire plasma, the electron number density,[6] n_e, is perhaps 10^{18} cm^{-3}, so $w_p = 5.6 \cdot 10^{13} s^{-1}$, and we easily satisfy $w >> w_p$.

TABLE 6

Data for Figure 6

Electron energy, E keV	w_{max} sec^{-1}	S_e Joule-m^2-sec	Equation for Fig.6
5	$7.5 \cdot 10^{18}$	$1.65 \cdot 10^{-59}$	11
10	$1.5 \cdot 10^{19}$	$8.48 \cdot 10^{-60}$	11
20	$3.0 \cdot 10^{19}$	$4.37 \cdot 10^{-60}$	11
50	$7.5 \cdot 10^{19}$	$1.89 \cdot 10^{-60}$	11
100	$1.5 \cdot 10^{20}$	$7.12 \cdot 10^{-61}$	12

We now consider the bremsstrahlung emitted by a plasma in which the electrons have a maxwellian velocity distribution. The bremsstrahlung spectrum is calculated by integrating equation 11 over the electron velocities, and the result is

$$X(w,T) = \frac{8\pi}{3\sqrt{3}} \frac{\bar{z}^2 e^6}{mc^3} \frac{1}{(4\pi\epsilon_0)^3} \frac{e^{-\hbar w/kT}}{kT} \bar{G}(w,T). \qquad (13)$$

Here T is the temperature and $\bar{G}(w,T)$ is the maxwell-averaged Gaunt factor and is given by Karzas and Latter.[15] As was the case for $G(w,v_o)$, $\bar{G}(w,T)$ is of order unity. Thus $X(w,T)$ depends on w mainly through the exponential factor and so has a much steeper variation than in the mono-energetic case (Fig. 6). Equation 13 should be valid[12] up to $w \simeq 13.6Z^2/\hbar$, or $\hbar w \simeq 74$ keV for $\bar{z} = 74$.

Applying equation 13 to the tungsten exploded-wire plasma, we set $\bar{z} = 74$, kT = 4.4 keV and 2.9 keV and obtain the spectra plotted in Fig. 7 . For the frequency range plotted here $\bar{G}$ remains constant at 1.2, so the spectra are purely exponential. They are the same as the straight lines sketched on Mosher's measured spectrum.[6]

The objective now is to discuss the flat portion of Mosher's spectrum which lies just to the right of the steep thermal portion, above about 8 keV. It is evidently due to a stream of fairly mono-energetic electrons (which we know yield flat spectra as in Fig. 6), and these electrons could be quite energetic since the discharge voltage is nearly 1 MV. We make use of the results of Kovrizhnykh[10] who gives an electron distribution function which is time dependent and applies in the case of a strong electric field. Here we assume a maxwellian distribution at

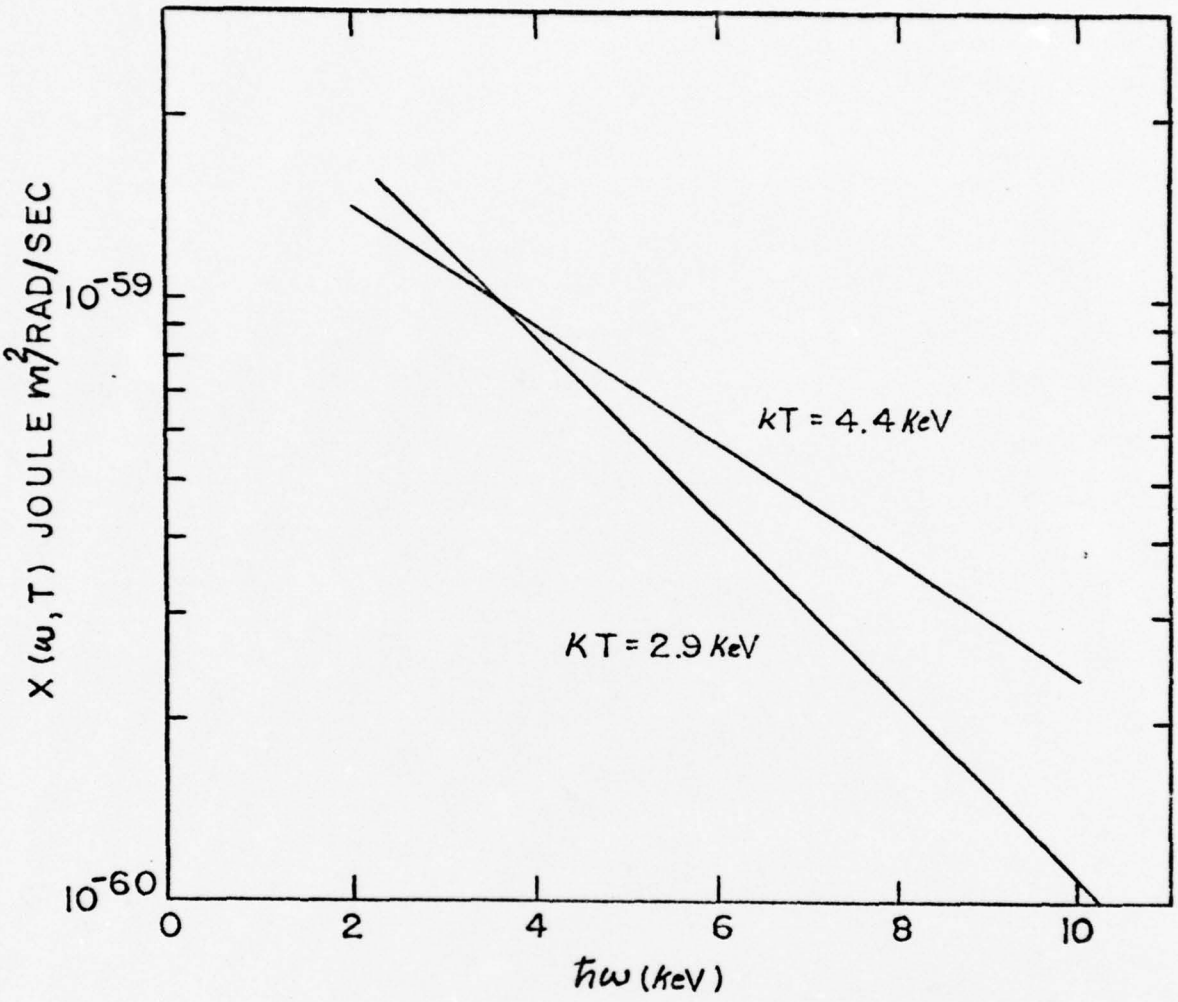

Figure 7. Thermal bremsstrahlung spectra for 2.9 and 4.4 keV temperatures

time t = 0,

$$f(\vec{v},\ t)\Big|_{t\,=\,0} = f_{max}(v_r,\ v_Z),$$

when the electric field is switched on. If collisions are neglected, solution of the Boltzmann equation for $t \geq 0$ gives[10]

$$f(\vec{v},\ t) = f_{max}(v_r, v_Z - \frac{e\xi}{m}\ t), \tag{14}$$

for an electric field, ξ, in the -Z direction. So the maxwellian shape moves in tact out along the v_Z axis at a rate $e\xi/m = \gamma$. The electrons thus accelerate toward the anode forming a hot beam, and the bremsstrahlung emitted as they encounter ions will be similar (although not identical) to a strictly mono-energetic or cold beam (Fig. 6).

The next step is to include collisions. If the collisions are assumed to have only a small effect, then

$$f(\vec{v},\ t) = f_{max}(v_r,\ v_Z - \gamma t)\{\ 1 +$$

$$\frac{\xi_k}{\xi}\left|\frac{\beta}{2v}\right.(v_Z - \gamma t)[v_Z - \gamma t)^2 + {v_r}^2]$$

$$+ \gamma t\ \frac{1 + \beta/2\ [(v_Z - \gamma t)^2 - {v_r}^2]}{v}$$

$$- \beta/2\ (v_Z - \gamma t)[{v_r}^2 + (v_Z - \gamma t)^2]^{1/2}$$

$$-(1 - \frac{\beta {v_r}^2}{2})\ \ell n(\frac{v + v_Z}{[{v_r}^2 + (v_Z - \gamma t)^2]^{1/2} + v_Z - \gamma t})]\},$$

(15)

where $f_{max}(v_r, v_Z - \gamma t) = n_e(\frac{\beta}{2\pi})^{3/2} e^{-1/2\beta[v_r^2 + (v_Z - \gamma t)^2]}$,

$\beta = m/kT$, and $\xi_k = 2\ 10^{-12}\ n_i \bar{z}^2/T_o$ V/cm with T_o in electron volts. This is Kovrizhnykh's result[10] modified by us to apply for any atomic number ($\bar{z}$) ion and any degree of ionization. Also, we have let $M/m \to \infty$. The function $f(\vec{v}, t)$ given by equation 15 is actually not too different from that in equation 14. Kovrizhnykh describes the differences. The region of validity of equation 15 depends on several plasma parameters according to the condition

$$\xi >> \xi_k \ell n\left(\frac{2\sqrt{2}\ e\ M\ E t}{m^{3/2}(kT)^{1/2}}\right).$$

Unfortunately, this shows that n_i must be $\lesssim 10^{14}$ cm^{-3} when we take, for the exploded wire, $\xi = 10^5$V/cm, $\bar{z} = 74$, $T_o = 4$keV, and $t_{max} = 10^{-10}$ sec. (t_{max} is discussed below.) Thus n_i is restricted to values less than the 10^{18}cm^{-3} reported by Mosher and so probably corresponds best to the region near the boundary of his plasma.

We have calculated the bremsstrahlung spectrum corresponding to the distribution function of equation 15 . The spectrum is given by

$$\bar{S}(w,t) = \int f(\vec{v}, t) n_i\ v\ \underset{o}{S}(v) G(w, v) d^3v. \qquad (16)$$

$\bar{S}(w, t)$ has units of watts/(m^3 - rad./sec).

A sizable amount of algebra is needed to put equation 16 into a form suitable for integration by computer. See the Appendix for details. The integrations have been done on an IBM 370 using Gauss-Laguerre quadrature as contained in the library routine DQG 32. The quantity

$S_o(v)G(w,v)$ is from equation 11. Grant[11] has calculated values for $G(w,v)$, and we have approximated these with the continuous function

$$G(w,v) = \begin{cases} \frac{\sqrt{3}}{\pi} \ell n\left(\frac{2}{1.78y}\right), & \text{for } y \leq 0.008 \\ \ell n(2.718 + 0.7716\, y^{-0.5809}), & \text{for } y > 0.008 \end{cases}$$

where $y = \frac{w}{4\pi\varepsilon_o} \frac{\bar{z}e^2}{mv^3}$

The distribution function and the spectrum depend on the time, t, so that one must determine a reasonable range for t. Taking a characteristic length for the exploded-wire plasma as ℓ = 1 cm, we obtain a maximum time, t_{max}, from

$$\ell = 1/2 \left(\frac{e\xi}{m}\right) t_{max}^2$$

Thus the range of t is $0 < t < t_{max} \sim 10^{-10}$ sec. for $\xi = 10^5$ V/cm. When $t = t_{max}$, the electron energy, $e\xi\ell$, is about 100 keV.

Fig. 8 shows $f(\vec{v},t)$ as a function of v_z with $v_r = 0$ for $t = 10^{-13}$, 10^{-12}, and $5 \cdot 10^{-11}$ sec. We have taken $= 10^5$ V/cm, $\bar{z} = 74$, $T_o = 4$keV, $n_i = 10^{14}$ cm^{-3}, and $n_e = 50 n_i^7$ Notice how $f(\vec{v},t)$ changes under the action of the electric field. It is shifted to the right and slightly distorted near its peak.

Fig. 9 shows $\bar{S}(w,t)$ for $t = 10^{-12}$, 10^{-11}, $5 \cdot 10^{-11}$, and 10^{-10} sec. for $n_i = 10^{14}$ and also 10^{12}. We see $\bar{S}(w,t)$ flatten out as t increases. Some wiggles appear in the spectrum for the larger n_i - evidently due to increased collisions. Mosher's measured (time-averaged) spectrum, with both the steep and the flat portions, might be imagined to arise from a distribution near the plasma boundary like the one we have calculated and a maxwellian distribution deeper inside where n_i is higher.

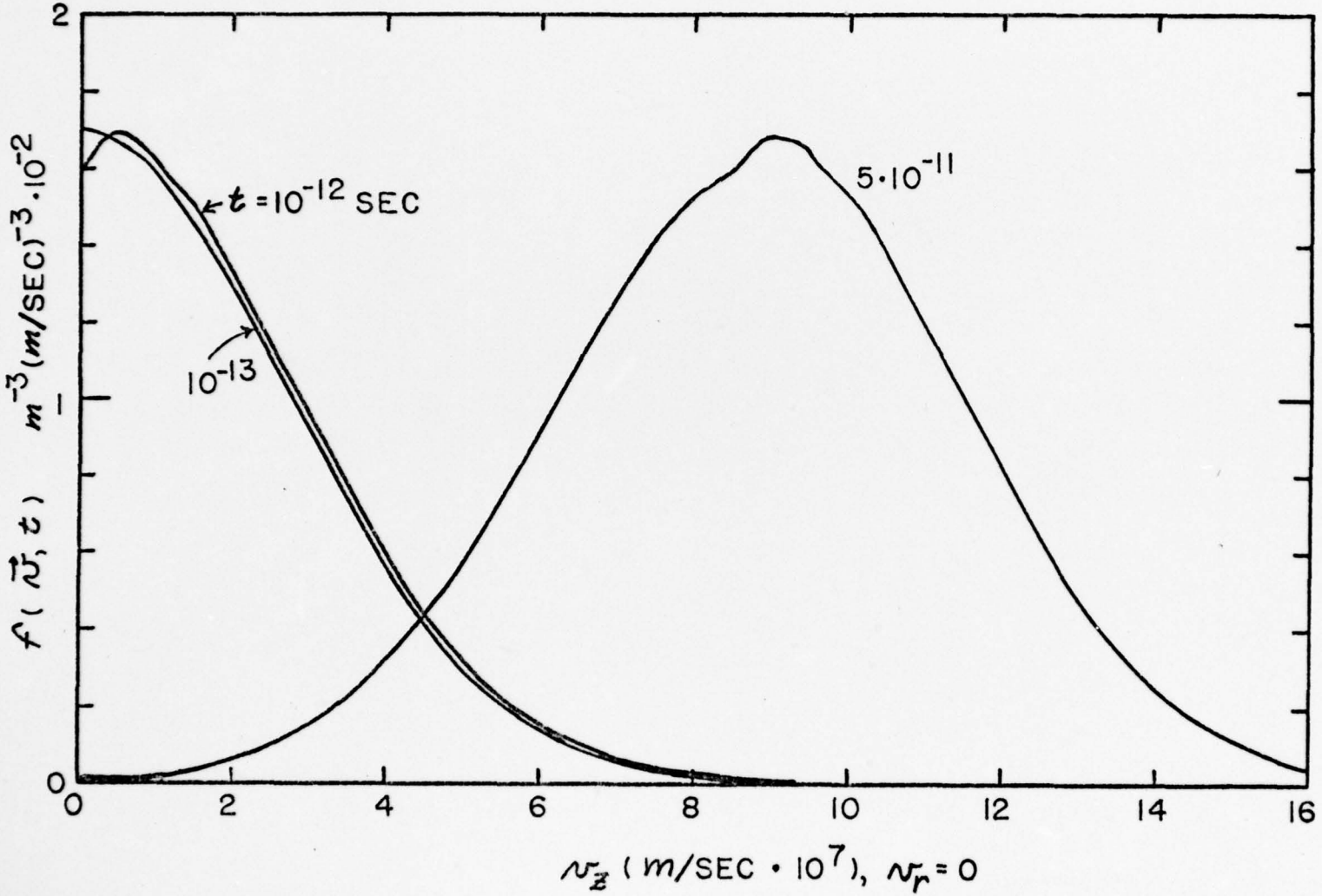

Figure 8. Electron velocity distribution for different times.

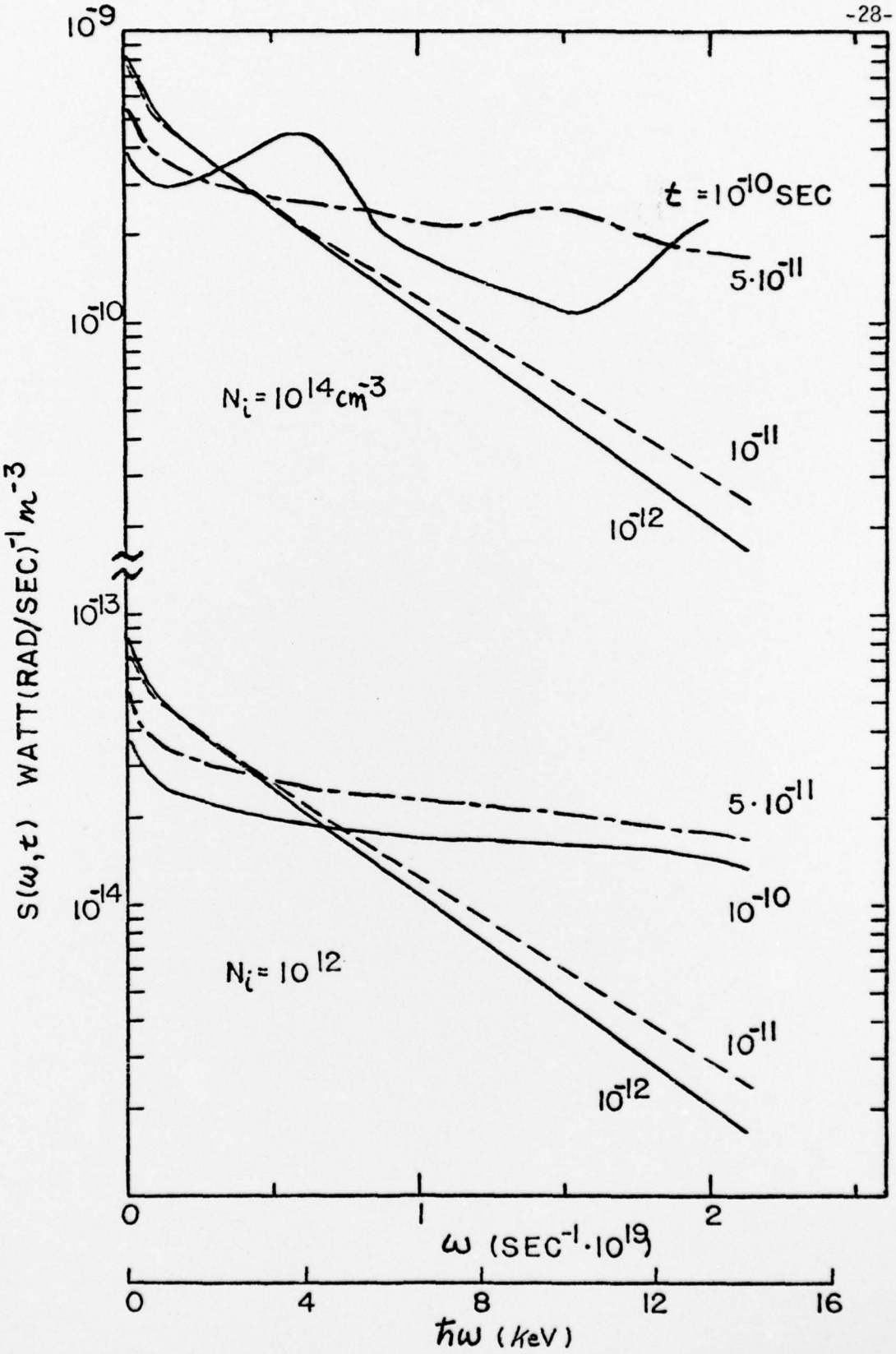

Figure 9. Bremsstrahlung spectra for time-varying electron velocity distributions

Of course one could plot $f(\vec{v},t)$ and $\overline{S}(w,t)$ for other values of the plasma parameters (lower T, for example). We have shown only the plots of interest for the exploded-wire plasma.

Finally, we note that for the distribution function we have used, (equation 15) most of the electrons may be classed as "runaway." The usual condition for electron runaway is that the energy gain of the electron in the electric field in one mean free path is larger than its thermal energy. This gives[5]

$$\xi_{runaway} = \frac{z^2 n_i}{2 \cdot 4 \cdot 10^{12} T_o} \quad V/cm$$

with T_o in eV. And for $n_i = 10^{14}$ cm^{-3}, $\xi_{runaway} = 57$ V/cm, so that with $\xi = 10^5$ V/cm we have $\xi >> \xi_{runaway}$. (If $n_i = 10^{18}$ though, $\xi = 10^5 < \xi_{runaway}$.)

APPENDIX

Integrations carried out by computer

On letting $v_z = v\cos\theta$, the electron distribution function given by equation (15) can be written as follows:

$$f(\vec{v},t) =$$

$$n_e(\beta/2\pi)^{3/2}\, e^{-\beta(a - b\cos\theta)} \left[1 + \frac{\varepsilon\gamma t}{\xi v}(1 - \beta v^2)\right.$$

$$+ \frac{\varepsilon\beta a}{2\xi}\cos\theta + (\gamma t - v\cos\theta)\frac{\varepsilon\beta}{2\xi}\sqrt{a - b\cos\theta}$$

$$\left.-\left(1 - \frac{\beta v^2}{2} + \frac{\beta v^2\cos^2\theta}{2}\right)\frac{\varepsilon}{\xi}\ell n\ \frac{v + v\cos\theta}{\sqrt{a - b\cos\theta} + v\cos\theta - \lambda t}\right] \qquad (A\text{-}1)$$

where

$$a = v^2 + \gamma^2 t^2,\ b = 2v\gamma t \text{ and } \varepsilon = 4\pi e^3\lambda n_i \bar{z}^2\beta/m.^{10}$$

The spectral intensity is given by

$$\bar{S}(w) = \int S(w,v)\, f(\vec{v},t)\, d^3v,$$

where

$$S(w,v) = S\, G(w,v)$$

$$d^3v = v^2 dv\, \sin\theta d\theta d\phi$$

and

$$S = \frac{1}{(4\pi\varepsilon_o)^3}\,\frac{16\pi}{3\sqrt{3}}\,\frac{n_i\bar{z}^2e^6}{m^2vc^3}\ .$$

$G(w,v)$ and S do not depend on θ and ϕ. On carrying out the angular integrations we get

$$I(v) = \int_0^{2\pi}\int_0^{\pi} f(\vec{v},t)\, \sin\theta d\theta d\phi$$

$$= 2\pi n_e(\beta/2\pi)^{3/2}\ [A(v)e^{-(\beta q^2)/2} + B(v)e^{-(\beta p^2)/2}$$

$$+ C(v)\int_p^q e^{-(\beta y^2)/2}\,dy + D(v)\int_p^q \frac{e^{-(\beta y^2)/2}}{(y+p)(y+q)}\,dy$$

$$+ E(v)\int_p^q \frac{y^2 e^{-(\beta y^2)/2}}{(y+p)(y+q)}\,dy + F(v)\int_p^q \frac{y^4 e^{-(\beta y^2)/2}}{(y+p)(y+q)}\,dy] \qquad \text{(A-2)}$$

where

$$p = v - \gamma t,\ q = v + \gamma t,\ \alpha = \beta v\gamma t,$$

$$A(v) = -\frac{1}{\alpha} - \frac{\varepsilon}{2\beta\xi}\left(\frac{1}{v^2} + \frac{1}{2\gamma^2t^2} + \frac{3}{2v\gamma t}\right)$$

$$+ \frac{\varepsilon}{\xi\beta\gamma t}\left(\frac{1}{v} + \frac{1}{\gamma t} + \frac{1}{\beta v\gamma^2t^2}\right)\ell n\left(1 + \frac{\gamma t}{v}\right)$$

$$B(v) = \frac{1}{\alpha} + \frac{\varepsilon}{2\beta\xi}\left(\frac{1}{v^2} + \frac{1}{2\gamma^2t^2} - \frac{3}{2v\gamma t}\right)$$

$$+ \frac{\varepsilon}{\xi\beta\gamma t}\left(\frac{1}{v} - \frac{1}{\gamma t} + \frac{1}{\beta v\gamma^2t^2}\right)\ell n\left(1 - \frac{\gamma t}{v}\right)$$

$$C(v) = \left(\frac{\varepsilon}{4\xi}\right)\left(\frac{1}{v} - \frac{v}{\gamma^2t^2} + \frac{3}{\beta v\gamma^2t^2}\right)$$

$$D(v) = \left(\frac{\varepsilon}{\xi}\right)\left[\frac{2}{\beta v} - v + \frac{1}{4v\gamma^2t^2}\left(a^2 - \frac{4a}{\beta} + \frac{8}{\beta^2}\right)\right]$$

$$E(v) = \left(\frac{\varepsilon}{\xi}\right)\left[\frac{2/\beta - a}{2v\gamma^2t^2}\right]$$

$$F(v) = \varepsilon/4\xi v\gamma^2t^2 \qquad \text{(A-3)}$$

For numerical integration it is necessary to modify the variable of integration y in the last four terms of I as follows:

Let $\sqrt{\beta/2}\ y = X$, $dy = \sqrt{2/\beta}\ dx$

Also define

$$q\sqrt{\beta/2} = XU \text{ and } p\sqrt{\beta/2} = XL.$$

Then

$$I = 2\pi n_e(\beta/2\pi)^{3/2}\left[A(v)e^{-(\beta q^2)/2} + B(v)e^{-(\beta p^2)/2}\right.$$
$$+ \frac{C(v)}{\sqrt{\beta/2}}\int_{XL}^{XU} e^{-X^2}\,dX + D(v)\sqrt{\beta/2}\int_{XL}^{XU}\frac{e^{-X^2}\,dX}{(X+XL)(X+XU)}$$
$$\left.+ \frac{E(v)}{\sqrt{\beta/2}}\int_{XL}^{XU}\frac{x^2e^{-X^2}dX}{(X+XL)(X+XU)} + \frac{F(v)}{(\beta/2)^{3/2}}\int_{XL}^{XU}\frac{X^4e^{-X^2}dX}{(X+XL)(X+XU)}\right]$$

The spectral intensity is given by

$$\bar{S}(w) = \int^{\infty} S\,G(w,v)\,I(v)\,dv$$

$$\frac{mv^2}{2} = \hbar w$$

Let us change the variable of integration v to Y as follows:

$$Y = \frac{mv^2}{2kT} - \frac{\hbar w}{kT}$$

Then

$$dY = \frac{m}{kT}\,vdv$$

and

$$v = \sqrt{\frac{2kT}{m}\left(Y + \frac{\hbar w}{kT}\right)}$$

Then

$$\bar{S}(w) = A_o\int_o^{\infty} G[w,v(Y)]\;I[v(Y)]e^{-Y}\,dY \qquad (A\text{-}4)$$

where

$$A_o = 2\pi n_e(\beta/2\pi)^{3/2}\,\frac{16\pi}{3\sqrt{3}}\,\frac{n_i z^2}{m^3c^3}\left(\frac{e^2}{4\pi\varepsilon_o}\right)^3 kT\,e^{-\hbar w/kT}$$

Before the right hand side of $\bar{S}(w)$ can be integrated numerically it is necessary to express the gaunt factor $g[w,v(Y)]$ in an analytical form. We have found that the following expression for $g[w,v(Y)]$ agrees very closely with Grant's results:

$$g(w,v) = \begin{cases} \frac{\sqrt{3}}{\pi} \ln\left(\frac{2}{1.78y}\right) & \text{for } y \leq .008 \\ \ln[2.7182818 + .771588\, y^{-.580864}] & \text{for } y > .008 \end{cases}$$

where

$$y = \left(\frac{w}{4\pi\varepsilon_o}\right)\left(\frac{\bar{z}e^2}{mv^3}\right) \qquad \text{(A-5)}$$

Because of the presence of the factor e^{-Y} in egn. (4) the integral can be evaluated numerically by using the fast and accurate Gauss-Laguerre guadrature scheme.

BIBLIOGRAPHY

1. Chase, W. G. and Moore, Exploding Wires, Plenum Press, Inc. New York, Vol. 1, 1959-Vol. 4, 1968.

2. Shipman, J. D., "Final Electrical Design Report of the GAMBLE II Pulse Generator," NRL Memoranda Report No. 2212.

3. Shipman, J. D., "The Electrical Design of the NRL GAMBLE II, 100 Kilo-Joule, 50 nanosecond, Water Dielectric Pulse Generator Used in Electron Beam Experiments," IEEE Trans. Nuclear Science Vol. NS-18, No. 4, p. 243, Aug. 1971.

4. Levine, L. S. and Vitkovitsky, "Pulsed Power Technology for Controlled Thermonuclear Fusion," IEEE Trans. Nuclear Science Vol. NS-18, No. 4, p. 255, Aug. 1971.

5. Mosher, D., Stephanakis, S. J., Hain, K., Dozier, C.M. and Young F. C., "Electrical Characteristics of High Energy-Density Exploded Wire Plasma" Annals of New York Academy of Sciences, Vol. 251, p. 632, May 8, 1975.

6. Mosher, D., Stepanaskis, J. J., Vitkovitsky, I. M., Dozier, C. M., Levine, L. S. and Nagel, D. J., "X-radiation from High-Energy-Density Exploded-wire Discharges," Appl. Phys. Lett. Vol. 23, No. 8, p. 429, 15 oct. 1973.

7. Mosher, David, "The Coronal Equilibrium of High Atomic Number Plasmas," NRL Memorandum Report 2563, March 1973.

8. Handbook of Chemistry and Physics, 49th Edition, Chemical Rubber Co. p. E228.

9. Spitzer, Lymon Jr., Physics of Fully Ionized Gases, Second Edition, No. 3, Interscience Publisher, 1962.

10. Kovrizhnykh, L. M., "Velocity distribution of electrons in a strong electric field," Soviet Physics JETP, 37(10), May, 1960, p. 989.

11. Grant, I. P., "Calculation of Gaunt Factors for Free-Free Transitions near positive ions," Month. Not., Roy. Astron. Soc., 118, 1958, p. 241.

12. Shkarofsky, I. P., T. W. Johnston and M. P. Bachynoki, "The Particle Kinetics of Plasmas," Addison-Wesley, 1966, Chapter 6.

13. Koch, H. W. and J. W. Motz, "Bremsstrahlung cross-section formulas and related data," Rev. Mod. Phys., 31, Oct. 1959, p. 920.

14. Jackson, J. D., "Classical Electrodynamics," John Wiley & Sons, 1962, chapter 15.

15. Karzas, W. J. and Latter, R., "Electron Radiative Transitions in a Coulomb field," Astrophys. J., Supp. Serv. 6, 1961, p. 167.

SECURITY CLASSIFICATION OF THIS PAGE (When Data Entered)

REPORT DOCUMENTATION PAGE

READ INSTRUCTIONS BEFORE COMPLETING FORM

1. REPORT NUMBER: AFOSR-TR-76-1105	2. GOVT ACCESSION NO.
3. RECIPIENT'S CATALOG NUMBER	
4. TITLE (and Subtitle): RADIATION GENERATION FROM EXPLODING WIRE	5. TYPE OF REPORT & PERIOD COVERED: Final rept.
	6. PERFORMING ORG. REPORT NUMBER
7. AUTHOR(s): M. G. Bhattacharya, J. P. Craig, T. F. Trost	8. CONTRACT OR GRANT NUMBER(s): AF-AFOSR-2830-76
9. PERFORMING ORGANIZATION NAME AND ADDRESS: Texas Tech University, Department of Electrical Engineering, Lubbock TX 79409	10. PROGRAM ELEMENT, PROJECT, TASK AREA & WORK UNIT NUMBERS: AF-9751-03, 61102F, 975103
11. CONTROLLING OFFICE NAME AND ADDRESS: AFOSR/NP, Bolling AFB, Wash DC 20332	12. REPORT DATE: 31 Aug 76
	13. NUMBER OF PAGES: 35
14. MONITORING AGENCY NAME & ADDRESS (if different from Controlling Office)	15. SECURITY CLASS. (of this report): Unclassified
	15a. DECLASSIFICATION/DOWNGRADING SCHEDULE

16. DISTRIBUTION STATEMENT (of this Report)

Approved for public release; distribution unlimited.

17. DISTRIBUTION STATEMENT (of the abstract entered in Block 20, if different from Report)

18. SUPPLEMENTARY NOTES

19. KEY WORDS (Continue on reverse side if necessary and identify by block number)

20. ABSTRACT (Continue on reverse side if necessary and identify by block number)

A theoretical investigation has been performed on the dual nature of the experimentally observed x-ray spectra emitted by high power exploded wire plasmas. The observed spectra consist of a steeply decreasing region for photon energies below about 8 KeV followed by a nearly constant region above this value. The region of steep decrease is the result of Bremsstrahlung from plasma electrons having a Maxwellian distribution. The constant region was considered as being caused by non-thermal high energy electrons. The constant region was investigated in more detail. They calculated first the Bremsstrahlung spectrum

DD FORM 1 JAN 73 1473 EDITION OF 1 NOV 65 IS OBSOLETE

UNCLASSIFIED 406 820

SECURITY CLASSIFICATION OF THIS PAGE (When Data Entered)

that would result from mono-energetic electrons of 5, 10, 20, 50 and 100 KeV incident on tungsten targets. All the spectra were found to have the same flat shape. The case of non-Maxwellian distribution of electrons was examined by using a distribution function appropriate to a homogeneous plasma in a strong electric field. After integration it was found that the spectrum changed from steep to flat as a function of time. It was concluded that a flat spectrum may arise through a distortion of the electron distribution function in a strong electric field.